Emission Control Science and Technology (2023) 9:166–176
https://doi.org/10.1007/s40825-023-00229-w

Influence of Asymmetric Channel Structure on Capture and Regeneration Process of Diesel Particulate Filter

Dong Tang[1] · Pengfei Zhang[1] · Yubin Han[1] · Yang Liu[1]

Received: 12 February 2023 / Revised: 13 June 2023 / Accepted: 14 July 2023 / Published online: 27 July 2023

Abstract

It is well known that diesel engines emit some particulate matter (PM); the simplest way to remove PM is to install diesel particulate filters (DPF). Asymmetric channel of DPF improves DPF performance by changing the relative size of inlet and outlet width to increase the carrying capacity for soot and ash. However, it is necessary to study the ratio of inlet to outlet channel width. In this study, the mathematics model of square asymmetric channel DPF is established to simulate the effects of different inlet and outlet channel width ratios (CRD) on pressure drop filtration efficiency and regeneration. The results verify that the capture efficiency decreased with the increase of CRD, and the capture efficiency could reach more than 99% after 200 s. With the increase of CRD, the total pressure drop of asymmetric channel DPF in clean state gradually increases. When the soot load is 6 g/L, the expansion pressure drop of DPF increases with the increase of CRD, but the total pressure drop decreases with the increase of CRD. The soot distribution in the asymmetric channel DPF tends to be thin at the front end and thick at the back end. The larger the CRD is, the smaller the thickness of the front soot is. In the process of regeneration, the DPF with larger CRD is easy to produce higher peak wall temperature, conducive to promoting the regeneration oxidation of soot.

Keywords Diesel engine · Diesel particulate filter (DPF) · Asymmetric channel · Capture · Regeneration · Pressure drop

Abbreviations

DPF	Diesel particulate filters
CRD	Width ratio of inlet and outlet channels of asymmetric channel of diesel particulate filter

Nomenclature

d_1	The side length of the inlet channel
d_2	The side length of the outlet channel
ΔP	Total pressure drop of DPF
ΔP_1	The pressure drop caused by the contraction at the inlet
ΔP_2	The pressure drop caused by the friction between the gas in the inlet channel and the wall
ΔP_3	The pressure drop caused by the gas passing through the soot cake layer
ΔP_4	The pressure drop caused by the gas passing through the ash layer
ΔP_5	The pressure drop caused by the gas passing through the DPF carrier wall
ΔP_6	The pressure drop caused by the friction between the gas and the wall in the outlet channel
ΔP_7	The pressure drop caused by the contraction of the outlet. In the formula,
$\xi_{contraction}$	Contraction pressure drop coefficient
$\xi_{expansion}$	Expansion pressure drop coefficient of the carrier, respectively; the coefficient usually varies from 0.3 to 5
U_{inlet}	The flow rate at the inlet, m/s
U_{outlet}	The flow rate at the inlet outlet, m/s
$U_{w,1}$	The flow rate of gas entering the soot layer, m/s
U_{w1-2}	The flow rate of gas entering the ash layer, m/s
$U_{w,2}$	The flow rate of gas entering the carrier wall, m/s
ρ_{inlet}	The gas density of gas entering the DPF, kg/m^3
ρ_{outlet}	The gas density after passing through the DPF, kg/m^3
ρ_w	The gas phase density in the substrate
ρ	The gas density inside the DPF, kg/m^3
μ	The viscosity of the gas inside the DPF, Pa s
D	The side length of the DPF channel, m
V_{trap}	The total volume of the DPF, m^3
Q	The volume flow rate of inlet, m^3/s
F	The pressure drop coefficient of the channel
L	The length of DPF channel, m

✉ Dong Tang
dtang@ujs.edu.cn

[1] School of Automobile and Traffic Engineering, Jiangsu University, Zhenjiang 212000, China

w_{soot}	The thickness of filter cake layer inside the DPF, m
w_{wall}	The wall thickness of DPF, m
w_{ash}	The ash thickness in the channel, m
β_{soot}	Forchheimer constant of DPF cake layer, 1/m
β_{wall}	Forchheimer constant of DPF wall, 1/m
β_{ash}	Forchheimer constant of the ash layer in the channel, 1/m
$k_{wall,\,i}$	The permeability of the DPF wall of the i discrete layer, m^2
$m_{engine-out}$	The mass of soot particulate entering the DPF exhaust gas, kg
Φ	The mass distribution coefficient of particles deposited on the surface of the tunnel
E_{cake}	The capturing efficiency of particulate in the soot layer inside the DPF
N_{cell}	The number of inlet channels
L_{eff}	Effective length of the channel, m
ρ_{cake}	The soot density of the cake layer in the channel, kg/m^3
T_w	The gas temperature of the filter wall
T_i	The gas temperature in the channel
T	The filter substrate temperature and its value is 860 K
h_i	The heat transfer by conduction (for forced convection along a channel)
h_c	The amount of heat transferred through conduction from the channel to the wall
c_g	The heat transfer coefficient of the filter wall and flow
c_p	The gas specific heat capacity
S	The total surface of the volume
k_p	The permeability of the particle
k_s	The permeability of the filter wall
μ_w	The dynamic viscosity of the gas through the wall
K_{thm}	The rate constant of the reaction, mol/L/s
S_p	The surface area in the substrate layer
Y_{oxygen}	The mass fraction of O_2 and its value is 0.1
A_T	The thermal frequency factor and its value is 1.43×10^6/s
E_T	The thermal activation temperature and its value is 139.46/(kJ mol^{-1})

1 Introduction

Compared with gasoline engine, the diesel engine has the advantages of high efficiency, better power performance, low fuel consumption, and strong reliability. It has been widely used in various fields such as large commercial vehicles, ships, engineering machinery, and so on [1]. However, diesel engines can emit harmful substances, including nitrogen oxides (NO_x), hydrocarbons (HC), particulate matter (PM), and so on which violates the requirements of advocating energy conservation, emission reduction, and environmental protection [2–4]. Therefore, many countries have promulgated and implemented strict emission regulations [5, 6]. At present, relying on the traditional in-cylinder purification technology of diesel engine is not sufficient to achieve effective PM reduction targets. The most widely used solution is the addition of diesel particulate filter (DPF). [7–9].

The interior of DPF is a porous honeycomb structure with one section open and one section blocked. The engine exhaust gas passes through the walls of the channel and is filtered and purified by the porous media, which adsorbs the particulates in the exhaust in the wall slits [10, 11]. A large number of studies have proved that the filtration efficiency of DPF can reach more than 90% [12–14]. However, the accumulation of large amounts of soot leads to a reduction in filter wall permeability and an increase in backpressure, which leads to a reduction in engine fuel efficiency and an increase in fuel consumption, so the captured PM must be regenerated by oxidation through the filter [15, 16]. To increase the soot capture volume and filtration area, an asymmetric channel DPF has been introduced, and the channel shape has been derived from octagonal channels in addition to the usual square channel. At present, a large number of scholars have studied the pressure drop and regeneration characteristics of asymmetric channel DPFs through experiments or the development of relevant mathematical models [17]. Lee et al. [18] adopted a one-channel mathematics model to predict the transient thermal response of the DPF. The effect of the ratio of length to width, cell density, the amount of soot loading on the temporal thermal response, and regeneration characteristics were investigated. They found that under "city driving mode," the maximum wall temperature of regeneration decreases with the increase of the ratio of length to width and the maximum temperature decreased with increasing cell density. Li Zhijun et al. [19] developed a DPF pressure drop model to compare the variation of DPF pressure drop in symmetrical and asymmetrical channel with uneven soot distribution and found that both had the lowest pressure drop in the case of thick soot in the front and thin soot in the back, but the DPF pressure drop was lower in the case of asymmetrical channel with the same soot distribution. Hidemasa Iwata et al. [20] studied the pressure drop and soot regeneration rate of asymmetric plugging layout diesel particulate filters (VPL-DPF) with different wall thickness; they found that the transient pressure drop of thick wall type DPF was lower than that of conventional DPF, but the soot oxidation rate during regeneration was lower. Zhang X et al. [21] studied the flow field distribution of the DPF with an asymmetric channel structure during the capture process and analyzed the pressure drop and gas velocity at the inlet and outlet. They found that the pressure drop of

the asymmetric DPF was higher than that of the symmetric channel, but when the soot load increased to a certain value, the pressure drop was just the opposite one. Ge Xiao et al. [22] proposed a novel type of asymmetric channel wall-flow filter, including the regular hexagonal and triangular channels, as well as the rectangular channels and developed corresponding mathematical models to study pressure drop characteristics. The results found that the novel asymmetric channel filter can effectively reduce the lifetime pressure drop by increasing the utilization ratio of the filtration wall and the filtration area.

In this study, based on a common square asymmetric channel DPF, the corresponding capturing, pressure drop, and regeneration models are developed. During the verification of regeneration model, the engine is used to first carry out soot accumulation on the DPF, and then the soot deposited DPF is loaded into the new system through off-line regeneration for regeneration verification. By varying the width ratio of inlet and outlet channels (CRD), the effect of the change in the ratio size on the DPF pressure drop, capturing efficiency, pressure drop composition, and soot distribution is investigated. The effect of the change in CRD on the regeneration characteristics of the DPF was analyzed in terms of peak wall temperature and regeneration rate.

2 Construction of the Computational Model

In this paper, GT-Power software is mainly used to simulate soot capture and regeneration process of DPF. The geometric parameters of the asymmetric channel filter were introduced before mathematical modeling was established. Figure 1 is an asymmetric DPF calculation unit. The ends of the inlet channel of the DPF and its outlet channel were blocked. Exhaust gas enters the outlet channel from the inlet channel through the wall surface, and then exits through the channel. As seen in Fig. 1, d_1 is the side length of the inlet channel, and d_2 is the side length of the outlet channel.

CRD (ratio of inlet to outlet channel width) of asymmetric channel DPF is:

$$CRD = \frac{d_1}{d_2} \tag{1}$$

Before establishing the DPF mathematics model, it is necessary to make reasonable assumptions to simplify the model. The specific assumptions are expressed as follows:

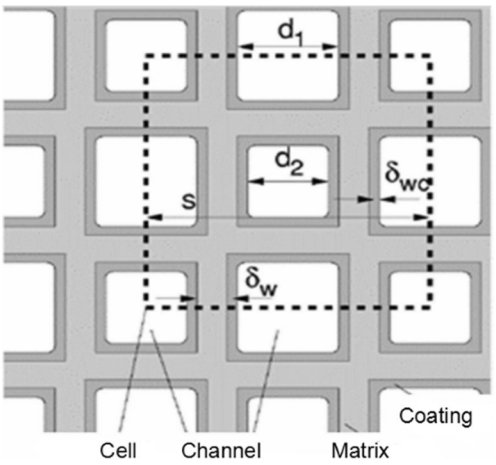

Fig. 1 The asymmetric DPF calculation unit

1. The physical parameters of all parts in the clean wall are consistent
2. The particulate matter in the exhaust gas only includes soot, without SOF, sulfate, etc.
3. Only considering laminar flow when the exhaust gas flows inside the DPF channel [23]

2.1 Pressure Drop Model of Asymmetric Channel DPF

The pressure drop is an important parameter in measuring the working performance of the DPF. Exhaust gas in through the inlet channel and out through the outlet channel via the porous media at the wall, and PM is filtered through this process and deposited on the wall surface. A pressure drop model based on Darcy's law can solve for the pressure loss caused by the DPF working process (including the soot loading and regeneration process) with the following equation [24, 25]:

$$\Delta P = \Delta P_1 + \Delta P_2 + \Delta P_3 + \Delta P_4 + \Delta P_5 + \Delta P_6 + \Delta P_7 \tag{2}$$

$$\Delta P_1 = \frac{\xi_{contraction}\rho_{inlet}U_{inlet}^2}{2} \tag{3}$$

$$\Delta P_2 = \frac{\mu Q}{2V_{trap}}\left(D + w_{wall}\right)^2 \frac{4FL^2}{3}\left(\frac{1}{\left(D - 2w_{soot}\right)^4}\right) \tag{4}$$

$$\Delta P_3 = \frac{\mu U_{w,1}\left(D - 2w_{soot} - 2w_{ash}\right)}{2k_{soot}} \ln\left(\frac{D}{D - 2w_{soot} - 2w_{ash}}\right) + \beta_{soot}\rho w_{soot}U_{w,1}^2 \tag{5}$$

$$\Delta P_4 = \frac{\mu_w U_{w1-2}}{2k_{ash}}\left(D - 2w_{ash}\right)\ln\left(\frac{D}{D-2w_{ash}}\right) + \beta_{ash}\rho w_{soot} U_{w,1-2}^2 \tag{6}$$

$$\Delta P_5 = \sum_i \left(\frac{\mu U_{w,2} w_{slab,i}}{k_{wall,i}} + \beta_{wall}\rho w_{slab,i} U_{w,2}^2\right) \tag{7}$$

$$\Delta P_6 = \frac{\mu Q}{2V_{trap}}\left(D + w_{wall}\right)^2 \frac{4FL^2}{3}\left(\frac{1}{D^4}\right) \tag{8}$$

$$\Delta P_7 = \frac{\xi_{expansion}\rho_{outlet} U_{outlet}^2}{2} \tag{9}$$

where ΔP_1 represents the pressure drop caused by the contraction at the inlet, ΔP_2 represents the pressure drop caused by the friction between the gas in the inlet channel and the wall, ΔP_3 represents the pressure drop caused by the gas passing through the soot cake layer, ΔP_4 represents the pressure drop caused by the gas passing through the ash layer, ΔP_5 represents the pressure drop caused by the gas passing through the DPF carrier wall, and ΔP_6 represents the pressure drop caused by the friction between the gas and the wall in the outlet channel. ΔP_7 represents the pressure drop caused by the contraction of the outlet. In the formula, $\xi_{contraction}$ and $\xi_{expansion}$ represent contraction pressure drop coefficient and expansion pressure drop coefficient of the carrier, respectively; the coefficient usually varies from 0.3 to 5. U_{inlet} and U_{outlet} indicates the flow rate at the inlet and the outlet respectively, m/s.

2.2 Soot Capture Model of Asymmetric Channel DPF

In the process of DPF capture, the soot is captured by the deep bed and intercepted by the wall pores of the DPF carrier channel. As the soot gradually increases, it enters the cake layer capture stage. The soot layer is covered on the wall of the DPF carrier channel, and the soot is burned after regeneration.

In the deep-bed capturing stage of DPF, the variation relationship of soot capture with time is as follows:

$$m_{wall}(t) = \sum_{i=1}^{N}\left[m_{in}(i,t)E(i,t-1)\right] \tag{10}$$

The mass of the soot cake layer after entering the filter cake capture stage can be expressed as follows:

$$m_{cake} = m_{engine-out}\cdot\Phi\cdot E_{cake} \tag{11}$$

The thickness of the soot cake layer can be expressed as:

$$w_{cake} = \frac{D_1 - \sqrt{{D_1}^2 - \frac{m_{cake}}{N_{cell}L_{eff}\rho_{cake}}}}{2} \tag{12}$$

2.3 Regenerative Soot Combustion Model of Asymmetric Channel DPF

Based on the assumptions, the governing equation of DPF regeneration process is shown below:

Mass balance:

$$\frac{d\left(\rho_i u_i D_i^2\right)}{dz} = (-1)^i 4 D_i \rho_w u_w \tag{13}$$

where $i = 1$ is the inlet channel; $i = 2$ is the outlet channel; ρ_i is the density of gas flow in the channel; ρ_w is the density of gas flow passing through the filter wall; u_i is the flow velocity in the channel, u_w is the filtration velocity of the air flow; D_i is the width of the channel, and z is axial direction.

Momentum balance:

$$\frac{d\left(p_i + \rho_i u_i^2\right)}{dz} = -\frac{\alpha\mu_i u_i}{D_i^2} \tag{14}$$

where p_i is the gas pressure in the channel; μ_i is the dynamic viscosity; α is the dimensionless frictional resistance coefficient.

Considering that the flow profile across the channel is not flat, the momentum convection term in the momentum balance should have a momentum flux correction factor [26, 27]:

$$\beta = \frac{1}{A\bar{u}^2}\int u^2 \mathrm{d}A \tag{15}$$

Gas energy balance:

$$\rho_i u_i \frac{D_i}{4} c_g \frac{dT_i}{dz} + \left[h_i + (-1)^i c_g \rho_w u_w\right]\left(T_w - T_i\right) = 0 \tag{16}$$

where T_w is the gas temperature of the filter wall; T_i is the gas temperature in the channel; h_i is the heat transfer by conduction (for forced convection along a channel); c_g is the heat transfer coefficient of the filter wall and flow.

The total heat transferred to the wall by the inlet [28]:

$$c_p S\rho u_{z2}\frac{\partial T_1}{\partial z} = \Pi\left(h_c - c_p\rho_w v_w\right)\left(T_w - T_1\right) \tag{17}$$

where c_p is the gas-specific heat capacity; S is the total surface of the volume; ρ is the gas density; h_c is the amount of heat transferred through conduction from the channel to the wall; on the perimeter Π, the normal component of velocity is v_w (pointing outward) for the inlet channel.

Darcy's law of pressure drop:

$$dp = \begin{cases} \frac{\mu_w}{k_p} u_w dx, x \in (0, w] \\ \frac{\mu_w}{k_s} u_w dx, x \in (w, w_s) \end{cases} \tag{18}$$

where k_p is the permeability of the particle; k_s is the permeability of the filter wall; μ_w is the dynamic viscosity of the gas through the wall; w is the thickness of the soot cake layer; w_s is the thickness of the filter wall.

During active regeneration, the temperature of DPF is higher than 600 °C, at which point the soot reacts with oxygen to generate CO and CO_2 [29]. The soot oxidation and filter regeneration model was constructed on the basis of the following global mechanism, considering thermal reaction kinetics.

Soot oxidation reaction:

$$C + \left(1 - f_{\mathrm{CO}}/2\right)O_2 \rightarrow f_{\mathrm{CO}}\mathrm{CO} + \left(1 - f_{\mathrm{CO}}\right)\mathrm{CO}_2 \tag{19}$$

$$f_{CO} = \frac{1}{1 + k_f \bullet y_{O_2}^{P_2} \bullet \exp\left(\frac{P_3}{R_0 \bullet T}\right)} \tag{20}$$

where f_{CO} is the selectivity of soot oxidize CO, which determines the concentration of CO and CO_2 as the soot is oxidized.

The soot oxidation rate over the above reaction is given by:

$$\dot{r}_{soot} = -K_{thm} S_p \rho_w Y_{oxygen} \frac{M_C}{M_{oxygen}} \tag{7}$$

Where the thermal reaction rates of progress is given by [30]:

$$K_{thm} = A_T \exp^{-\left(\frac{E_T}{T}\right)} \tag{8}$$

In the preceding equations, M_C is the molecular weight of soot; M_{oxygen} is the molecular weight of oxygen; S_p is the surface area in the substrate layer; Y_{oxygen} is the mass fraction of O_2, and its value is 0.1; ρ_w is the gas phase density in the substrate; K_{thm} is the rate constant for thermal reaction; A_T is the thermal frequency factor, and its value is 1.43×10^6/s; E_T is the thermal activation temperature, and its value is 139.46/(kJ mol^{-1}); T is the filter substrate temperature, and its value is 860 K.

3 Model Validation

According to the user manual of GT-POWER, the calibration of the soot accumulation model mainly involves three factors: the permeability constant controls the pressure drop at the turning point from deep bed filtration to cake filtration, which usually varies in the range of 0.85~0.95 (constant without unit); the soot accumulation density of the filter wall varies in the range of 8~20 kg/m^3, and it controls the slope of pressure drop curve with respect to time during deep bed passing. The cumulative density of soot layer controls the slope of the pressure drop curve of cake filtration stage in relation to time. Since the cumulative density of soot can be expressed by the formula including the porosity of soot layer, the porosity of soot layer is taken as the parameter to be calibrated in the calibration process, and its variation range is 0.56~0.96.

Table 1 The fundamental parameters of the DPF

Parameter	Unit	Value
Structure		Asymmetric
Width of the filter	mm	143
Length of the filter	mm	178
Cell density	cpsi	300
Porosity	/	0.48
Inlet/outlet channel length	mm	1.4/1.05
Thermal conductivity	W/(m K)	0.85
Filter density	kg/m^3	1300

Table 2 Parameters of diesel engine

Specifications	Parameters
Displacement (L)	2.499
Cylinder width × stroke (mm)	93 × 92
Compression ratio	17
Calibration power (kw/r·min^{-1})	110/3600
Maximum torque/speed (N m/r·min^{-1})	320/1800–2000

The back pressure of clean DPF depends on its wall permeability k_w. By modifying the wall permeability parameter of the model, the relationship between simulated pressure drop and exhaust flow rate is close to the test results, which verifies the reliability and accuracy of the pressure drop model.

Clean and soot-free asymmetric channel DPF was selected to adjust engine working conditions, so that the mass flow rate of exhaust gas through DPF varied in 50–200 kg/h with little temperature difference, and the inlet temperature of DPF was about 490 K. The main parameters of DPF are shown in Table 1. Table 2 shows the main parameters of the diesel engine. The comparison between the measurement value and the simulated value is shown in Fig. 2. When the wall permeability k_w is 3×10^{-13} m^2, the maximum relative error between the simulated value and the measurement value is less than 5%, which indicates that the established pressure drop model is relatively close to the actual test situation and has certain reliability and accuracy.

Since the exhaust parameters of the diesel engine are unstable during operation, in order to reduce the influence of factors such as diesel exhaust parameters, the verification experiment in this paper adopts the offline regeneration method, and the aged filter (DPF after soot capture) was put into the built system for regeneration to achieve accurate control of environmental conditions. While verifying the

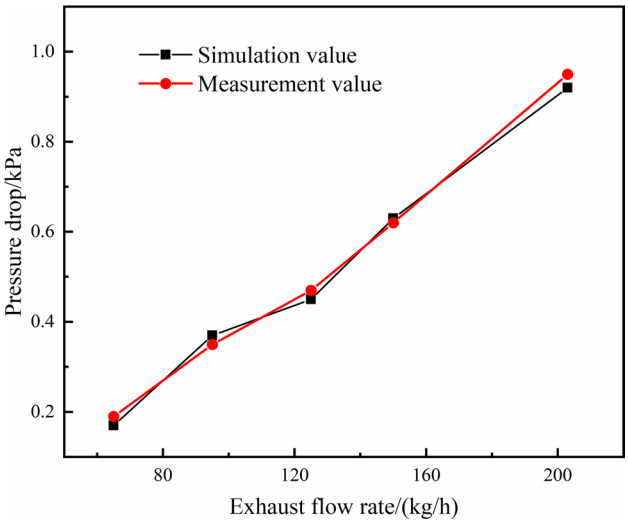

Fig. 2 DPF pressure drop simulation value and measurement value change with exhaust flow rate

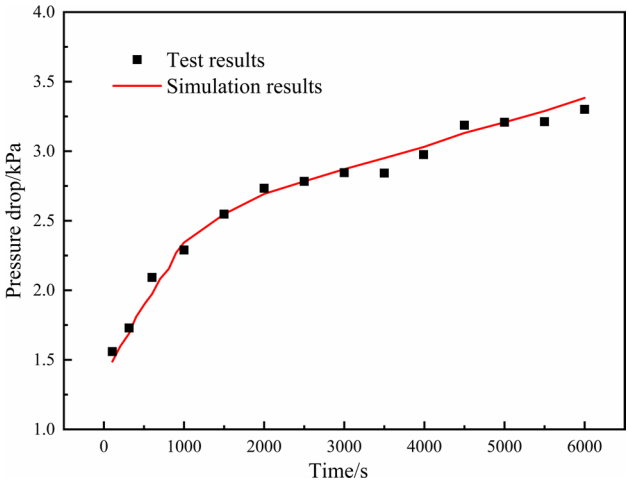

Fig. 3 Comparison of simulated and experimental values of DPF pressure drop

feasibility of the regeneration scheme, the experiment results can be used as a reference for the validation of chemical reaction kinetic parameters. The soot filtration experiment was carried out in the exhaust environment of a high-pressure common rail four-cylinder diesel engine to obtain the filter loading required for the offline regeneration experiment. The main material used for DPF was silicon carbide. The main parameters of DPF and diesel engine are shown in Tables 1 and 2. The filtration process was carried out under the condition of 1800 r/min and 50% load rate of the diesel engine. During the capture process, the relationship between pressure drop and time was recorded. The engine is only used for soot loading, not for regeneration studies.

Based on the soot capture experiment, the pressure drop data obtained by the experiment was compared with the simulated value, and the value of the optimization function was set as the sum of squares of the difference between the two. The solution of the optimization function at the minimum value was obtained, and the permeability constant P was 0.9, the soot density on the wall of the DPF ρ_{wall} was 22 kg/m^3, and the porosity of the soot layer ε_{soot} was 0.83 (all three values are fitting parameters). Figure 3 shows the comparison results between the obtained DPF simulated pressure drop and the experiment measured values. It can be seen that the DPF pressure drop curve is similar to the experiment results, indicating that the calibrated DPF capture model is more accurate.

The offline regeneration experiment system diagram is shown in Fig. 4. These include gas heaters, temperature control boxes, oxygen sensors, differential pressure gauges, thermocouples, and other devices. The intake gas is O_2/N_2 mixture. Before the experiment, N_2 was added to discharge the original gas in the pipeline. During the experiment, the intake air was heated to 858 K by a temperature-controlled gas heater to reach the temperature required for regeneration. The intake gas ratio was changed by adjusting the valves and the flow meter, and the total inlet flow rate was 1400 L/min. The pressure drop data can be obtained by means of differential manometer.

As shown in Fig. 5, when mass concentration of initial soot in DPF was 6.5 g/L, the error in predicted backpressure was not more than 7%. Therefore, the established DPF model is relatively accurate and can reflect the experiment results better. Based on this mathematical model, further effect analysis on regeneration of DPF can be conducted.

4 Results and Discussion

4.1 Influence of CRD on the Capture Process

In order to study the influence of asymmetric carriers on DPF pressure drop, DPF carriers with inlet to outlet channel width ratios of 1, 1.1, 1.2, 1.3, and 1.4 are selected to calculate the change in DPF pressure drop and capture efficiency with time. The mass concentration of soot in exhaust is 1.7 E^{-4} kg/m^3, the exhaust temperature is 550 K, and the exhaust flow rate is 200 kg/h. The DPF pressure drop of different inlet to outlet channel width ratios varied with time, as shown in Fig. 5.

As can be seen in Fig. 6a, at the beginning of the capture, with the CRD of the DPF increases from 1 to 1.4, the initial pressure drop of the DPF increases from 1.4 to 1.9 kPa. The increase of CRD will lead to the decrease of the volume of the outlet channel; consequently, the wall permeability of DPF becomes poor, and the backpressure across the DPF increases. During the period of 0–250 s of capture

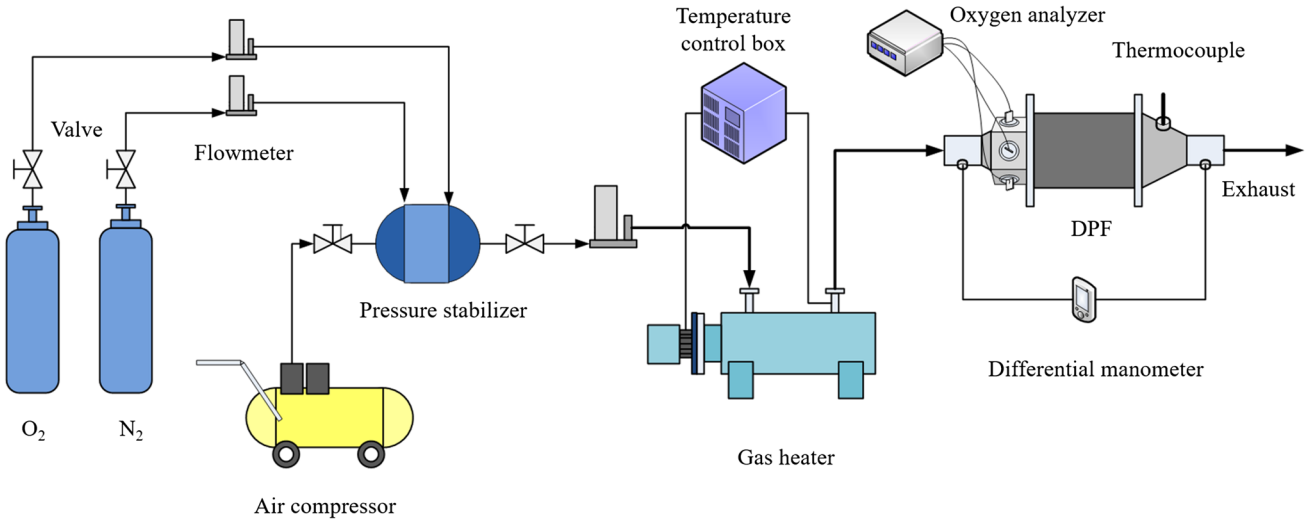

Fig. 4 Offline regeneration system

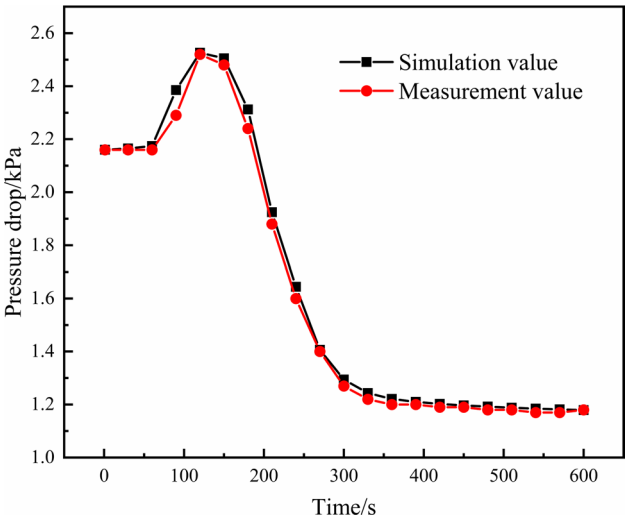

Fig. 5 Simulation value and measurement value of pressure drop of DPF

process, the five filters are in the deep-bed filtration stage, the pressure drop increases rapidly, and the growth trend is consistent. However, the increase of CRD will increase the surface area of the inlet channel and increase the amount of soot that can be carried inside the wall. Therefore, the DPF deep-bed filtration stage last longer when the CRD is 1.4. At 500–2400 s of the capture process, the soot mass in the DPF wall reached saturation, and soot starts to accumulate on the inner surface of the channels. Compared with the saturated carrier wall, the soot layer permeability is larger, so the pressure drop of DPF increases slowly with time. Due to the large surface area of the asymmetric filter inlet channel, the thickness of soot accumulated in the channel is thin, and the rate of increase of the DPF pressure drop is also smaller.

Figure 6 b shows the relationship between the capture efficiency of DPF carriers with different CRD over time. When DPF was clean, the capture efficiency decreased with the increase in CRD. When CRD increased, the carrier area that exhaust gas can pass through from the intake channel to the outlet channel decreases, that is, the actual filtration volume decreases. At 0–500 s of the capture process, soot accumulation within the carrier surface until the saturated state, five kinds of DPF capture efficiency is increased rapidly. With the increase in the CRD, the capture efficiency curve of the DPF deep-bed filtration stage migrated downward as a whole.

4.2 Pressure Drop Composition

In order to explore the reasons for the large pressure drop of asymmetric DPF in the initial stage of capture, the pressure drop composition in the clean state of DPF should be studied first. The pressure drop in DPF in the clean state is mainly composed of five parts: inlet channel pressure drop, outlet channel pressure drop, inlet channel contraction pressure drop, outlet channel expansion pressure drop, and wall pressure drop. Set the inlet flow as 200 kg/h, the initial soot load as 0 g/L, exhaust temperature as 550 K, filter cell density as 300 cspi, and wall thickness as 9 mil. The DPF length is 178 mm. The pressure drop composition of asymmetric DPF was investigated.

Figure 7 shows the composition of the total backpressure across a DPF at different inlet and outlet channel width ratios in the clean state. It can be seen from the figure that, in the clean state, the inlet channel contraction pressure drop and the outlet channel expansion pressure drop were small, accounting for only about 3% of the total pressure drop. The pressure rises with the flow expansion at the exit of a filter.

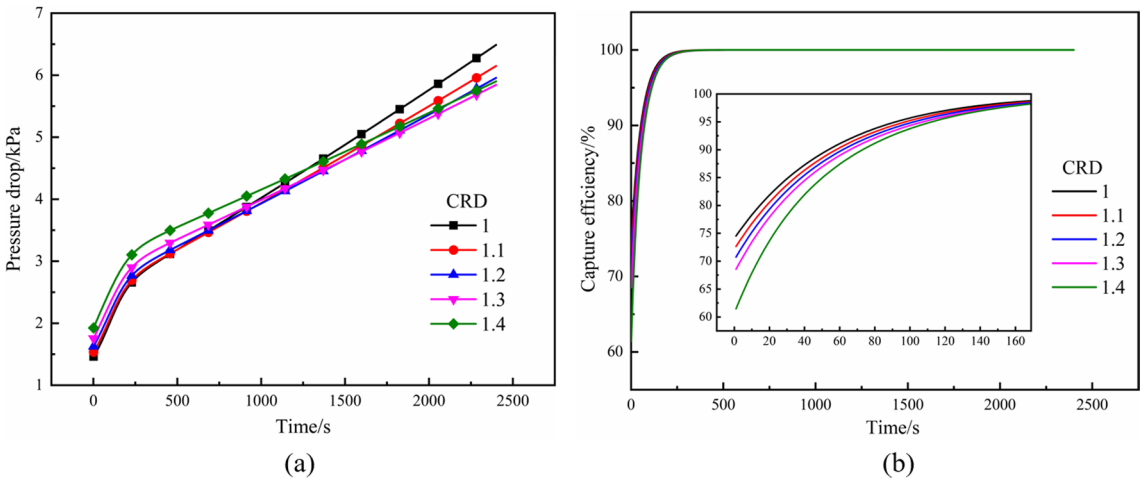

Fig. 6 Pressure drop (**a**) and capture efficiency (**b**) of DPF with different CRD over time

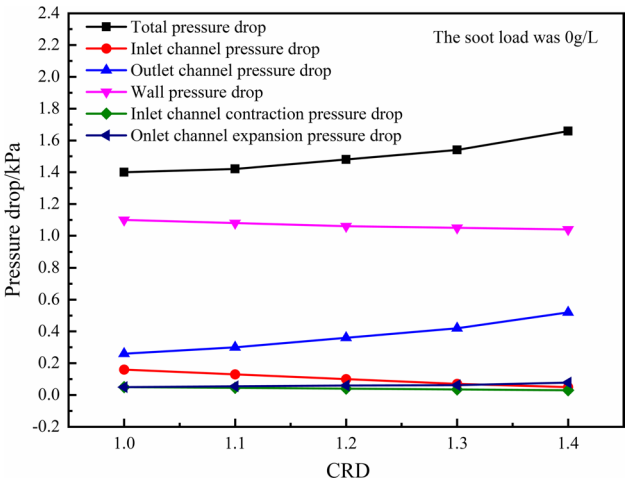

Fig. 7 Pressure drop composition of DPF with different proportion of inlet and outlet in clean state

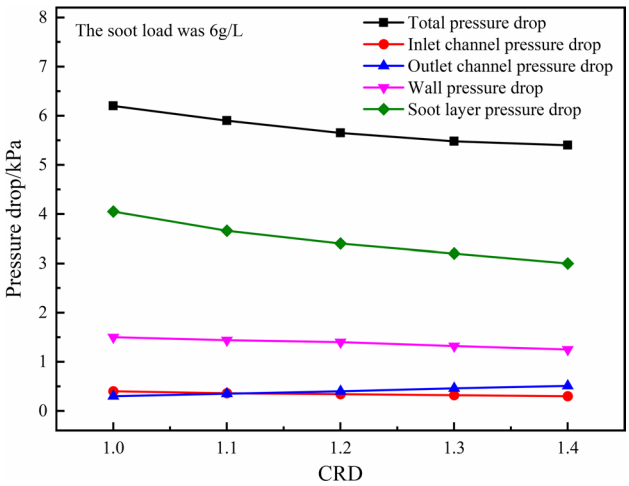

Fig. 8 The pressure drop of the DPF with different CRD when the soot load was 6 g/L

With the increase of the CRD, the inlet channel side length increased, and the outlet channel side length decreased. Therefore, the inlet channel pressure drop and inlet channel contraction pressure drop gradually decreased, while the outlet channel pressure drop and outlet channel expansion pressure drop gradually increased. It can also be seen from the figure that the wall pressure drop accounted for a higher proportion of the total pressure drop, and with the increase of CRD, the total area of the filter channel wall will increase, resulting in a small decrease in the wall pressure drop [22]. When the CRD is 1.4, the vent passage pressure drop rose greatly, resulting in a larger increase in the total pressure drop of DPF. Therefore, the total pressure drop of DPF will increase with the increase of CRD in the clean state.

Figure 8 shows the pressure drop composition of DPF with different CRD when soot load was 6 g/L, and the soot is uniformly distributed within the DPF. As can be seen from the figure, when the soot load was 6 g/L, the total pressure drop of DPF decreased from 6.2 to 5.4 kPa as the CRD increased from 1 to 1.4. The changed rule of DPF is the same as that in the clean state. With the increase of CRD, the pressure drop at inlet channel and inlet channel contraction decreases gradually, while the pressure drop at outlet channel and outlet channel expansion increases gradually. However, different from the composition of clean DPF, the soot layer pressure drop of DPF under the condition of 6 g/L soot load accounted for a large proportion of the total pressure drop. Since the increase in CRD can increase the internal surface area of the intake passage and reduce the thickness of the captured soot layer, the pressure drop of the soot layer decreases, and the decrease amplitude is larger than that of the pressure drop in the air vent. Therefore, in

the clean state, the pressure drop of asymmetric channel filter is larger than that of symmetric channel filter, but when the internal soot load of the carrier is large, the pressure drop of asymmetric channel filter is smaller.

4.3 Soot Distribution in the Channel

In the cake trapping stage, the captured soot was distributed on the inner surface of the intake passage. In order to study the distribution of soot in DPF with different CRD, the thickness of soot in the axial of DPF was simulated and calculated. Set the inlet flow as 200 kg/h, the initial soot load as 6 g/L, exhaust temperature as 550 K, filter cell density as 300 cspi, and wall thickness as 9 mil. The DPF length is 178 mm. Figure 9 shows the axial soot deposition thickness of DPF with different CRD when the soot load was 6 g/L. The axial relative position $s = \frac{X}{L}$, X represents the distance between the monitoring point and the DPF entry section, and L represents the total length of the DPF.

As can be seen from Fig. 9, soot presents concave distribution in the DPF. The thickness of soot deposited at the front and back ends of the carrier axis was larger, while the thickness deposited at the middle of the axis was smaller. As shown in Fig. 10, with the increase of CRD, the actual filtration area of DPF increased, and the overall thickness of the soot layer of the channel decreased. As the thickness of the soot layer in the channel decreases, the soot floating on the wall tends to move along with the exhaust flow, aggravating the non-uniformity of the axial distribution of the soot, resulting in a large difference between the thickness of the back-end soot and that of the front-end soot, which is not conducive to the regeneration process of DPF.

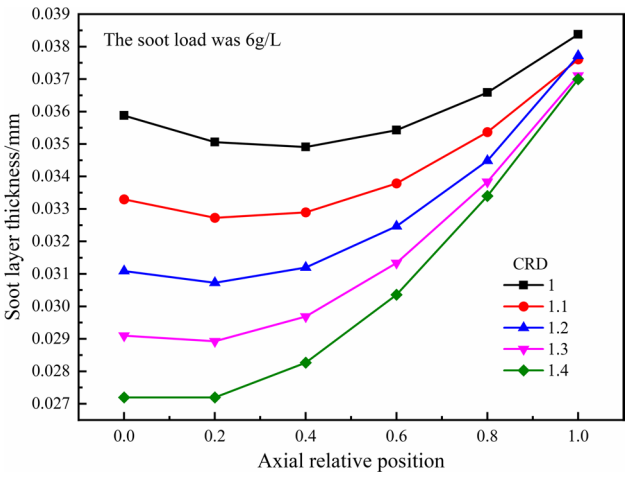

Fig. 9 The axial soot thickness of the DPF with different CRD when the soot load was 6 g/L

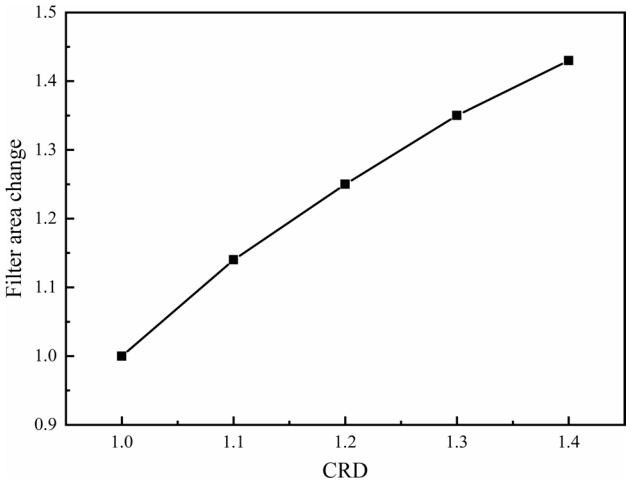

Fig. 10 Effect of CRD on filtration area

4.4 Effect of CRD on Regeneration Process

Due to the special design of inlet and outlet of asymmetric channel will affect the regeneration process. In this paper, the influence of asymmetric structure on the regeneration process of DPF is investigated on two bases, which are wall peak temperature and regeneration rate. The width and length of the DPF are set to 145 mm and 178 mm, the exhaust flow rate is 50 kg/h, and the exhaust temperature is 860 K. The initial soot load was 25 g. The selected filter CRD is 1, 1.2, and 1.4, respectively. The peak wall temperature and regeneration rate during regeneration process are shown in Fig. 11.

It can be seen from Fig. 11a that the symmetric DPF reached the peak wall temperature of 1230 K at 220 s, DPF with CRD of 1.2 reached the peak wall temperature of 1308 K at 190 s, and DPF with CRD of 1.4 reached the peak wall temperature of 1412 K at 170 s. Therefore, when the DPF of larger CRD was regenerated, a higher peak wall temperature was generated, and the peak temperature appeared earlier. The logical explanation for this phenomenon is that with the increase of CRD, the volume of the outlet passage decreased, which was not conducive for the flow of exhaust gas in DPF, resulting in slower heat loss from soot oxidation. In addition, the larger the CRD, the larger the contact area between gas and soot, which is more conducive to the combustion and oxidation of soot. The more intense the oxidation, the higher the temperature, the faster the combustion speed and the full oxidation, so the peak temperature increases with the increase of CRD. The faster the rate of oxidation and combustion, the faster the temperature rises.

Figure 11 b shows the change of soot load mass in DPF over time. It can be seen from the figure that at the early stage of regeneration, the soot load of asymmetric DPF with CRD of 1.4 began to decline first, and the trend of decline was the

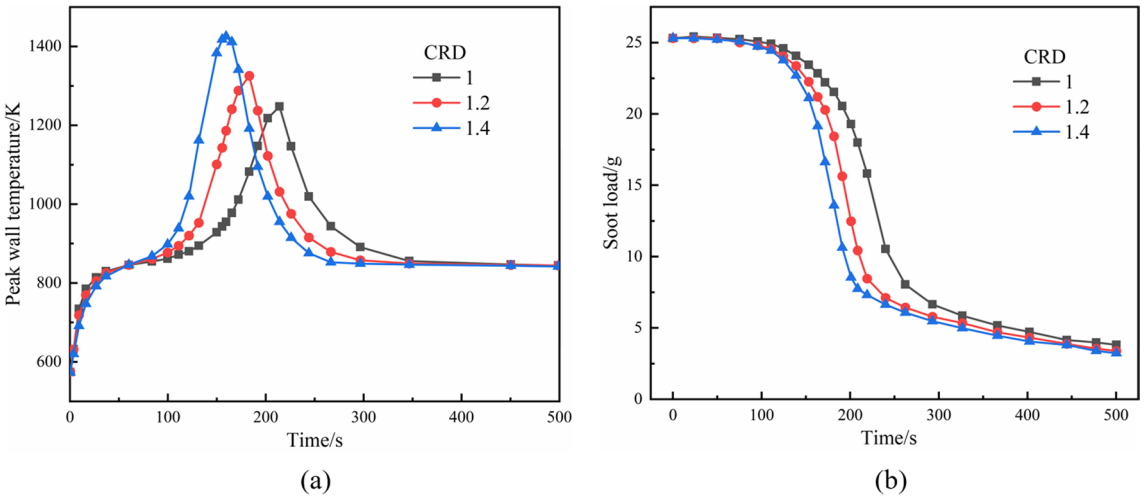

Fig. 11 Peak wall temperature (**a**) and the change of soot load mass (**b**) during DPF regeneration with different CRD

most rapid. That is, the regeneration rate was faster. After the end of the regeneration process, the residual soot in DPF carrier with CRD of 1.2 and 1.4 was smaller. The increase in CRD increased the area of the soot layer on the inlet channel surface and the contact area with the exhaust. In the process of regeneration, due to the slow heat discharge from asymmetric channel filter, there was more heat exchange between exhaust and carrier wall, resulting in faster regeneration rate and increase in the overall regeneration efficiency.

5 Conclusions

Due to the serious environmental pollution, it is important to study and optimize the capture and regeneration performance of DPF. In this paper, the regeneration and soot models of asymmetric DPF have been established, verified, and analyzed. The main conclusions are as follows.

1. In the early stage of capture, the initial pressure drop rises from 1.4 to 1.9 kPa as the CRD goes from 1 to 1.4. This indicates that the pressure drop of asymmetric channel DPF is higher than that of symmetric channel DPF. The capture efficiency of asymmetric channel DPF decreases with the increase of CRD, but the final capture efficiency can reach more than 99%.
2. In the clean state of DPF, with the increase of CRD, the inlet channel pressure drop and wall pressure drop decrease, but the total pressure drop increases. When the DPF soot load is 6 g/L, the pressure drop decreases except for the increase of the outlet channel pressure drop. In the axial position of DPF, the soot is thick at both ends and thin in the middle. With the increase of CRD, the actual filter area of DPF increases, and the total thickness of the soot layer decreases.
3. The increase of CRD has a certain effect on the regeneration performance of asymmetric DPF, and the regeneration peak temperature can be reached quickly during regeneration, which promotes the oxidation and regeneration of soot. With the increase of CRD, the regeneration oxidation rate of soot increased, and the residual soot was less.

Author Contributions Dong Tang: conceptualization, methodology. Pengfei Zhang: visualization, writing—original draft. Yubin Han: software, analysis of data. Yang Liu: supervision.

Funding This study was financially supported by the National Natural Science Fund of China (No. 51876085) and Open Fund of State Key Laboratory of Internal Combustion Engine Reliability in China (skler-202105).

Data Availability All relevant data are within the manuscript and available from the corresponding author upon request.

Declarations

Ethics Approval Not applicable.

Consent to Participate The work described has not been published before; the work is not under consideration for publication elsewhere; and its publication has been approved by all co-authors. Its publication has been approved by the responsible authorities at the institution where the work is carried out.

Consent for Publication All authors have agreed with the content, and all have given explicit consent to publish.

Compliance with Ethical Standards The authors declare no competing interests.

References

1. Zhou, L., Gao, Z.Y.: Engine Science, pp. 1–10. China Machine Press, Beijing (2010)
2. Chen, K., Martirosyan, K.S., Luss, D.: Temperature gradients within a soot layer during DPF regeneration. Chem. Eng. Sci. **66**, 2968–2973 (2011). https://doi.org/10.1016/j.ces.2011.03.037
3. Liu, P.: Chemical analysis of various fractions of diesel exhaust particulates from modern diesel engines and an investigation on bio-toxicity of soluble organic fractions. M.Sc. Thesis. Tianjin University, Tianjing (2004)
4. Szabados, G., Bereczky, Á., Ajtai, T., Bozóki, Z.: Evaluation analysis of particulate relevant emission of a diesel engine running on fossil diesel and different biofuels. Energy. **161**, 1139–1153 (2018). https://doi.org/10.1016/j.energy.2018.07.154
5. Johnson, T., Joshi, A.: Review of vehicle engine efficiency and emissions. SAE Int. J. Engines. **11**(6), 1307–1330 (2017)
6. Selleri, T., Melas, A.D., Joshi, A., Manara, D., Perujo, A., Suarez-Bertoa, R.: An overview of lean exhaust deNO$_x$ aftertreatment technologies and NO$_x$ emission regulations in the European Union. Catalysts. **11**, 404 (2021). https://doi.org/10.3390/catal11030404
7. Wang, K., Liu, S., Li, R., Wang, Z.: Analysis of the effect of particle–wall collision process in DPF on the spatial structure of smoke cake layer. Environ. Sci. Pollut. Res. **28**, 26895–26905 (2021). https://doi.org/10.1007/s11356-020-12277-8
8. Rodríguez-Fernández, J., Oliva, F., Vázquez, R.A.: Characterization of the diesel soot oxidation process through an optimized thermogravimetric method. Energy Fuels. **25**, 2039–2048 (2011). https://doi.org/10.1021/ef200194m
9. Tan, P., Cao, C., Hu, Z., Lou, D.: Modeling of soot fragmentation that proceeds in a catalyzed diesel particulate filter of a diesel engine. Chem. Eng. J. **375**, 122110 (2019). https://doi.org/10.1016/j.cej.2019.122110
10. Ye, J., E, J., Peng, Q.: Effects of porosity setting and multilayers of diesel particulate filter on the improvement of regeneration performance. Energy. **263**, 126063 (2023). https://doi.org/10.1016/j.energy.2022.126063
11. Zhang, B., Gong, J., E, J., Li, Y.: Failure recognition of the diesel particulate filter based on catastrophe theory. Can. J. Chem. Eng. **94**, 596–602 (2016). https://doi.org/10.1002/cjce.22424
12. Wang, X., Wang, Y., Bai, Y.: Oxidation behaviors and nanostructure of particulate matter produced from a diesel engine fueled with n-pentanol and 2-ethylhexyl nitrate additives. Fuel. **288**, 119844 (2021). https://doi.org/10.1016/j.fuel.2020.119844
13. Meng, Z., Chen, C., Li, J., Fang, J., Tan, J., Qin, Y., Jiang, Y., Qin, Z., Bai, W., Liang, K.: Particle emission characteristics of DPF regeneration from DPF regeneration bench and diesel engine bench measurements. Fuel. **262**, 116589 (2020). https://doi.org/10.1016/j.fuel.2019.116589
14. Meng, Z., Li, J., Fang, J., Tan, J., Qin, Y., Jiang, Y., Qin, Z., Bai, W., Liang, K.: Experimental study on regeneration performance and particle emission characteristics of DPF with different inlet transition sections lengths. Fuel. **262**, 116487 (2020). https://doi.org/10.1016/j.fuel.2019.116487
15. Wang, H., Ge, Y., Tan, J., Hao, L., Wu, L., Yang, J., Du, Q., Zhang, H., Huang, Y., Chen, Y., Li, X., Peng, Z.: Ash deposited in diesel particular filter: a review. Energy Sources Part Recovery Util. Environ. Eff. **41**, 2184–2193 (2019). https://doi.org/10.1080/15567036.2018.1550539
16. Fang, J., Zhang, Q., Meng, Z., Luo, Y., Ou, J., Du, Y., Zhang, Z.: Effects of ash composition and ash stack heights on soot deposition and oxidation processes in catalytic diesel particulate filter. J. Energy Inst. **93**, 1942–1950 (2020). https://doi.org/10.1016/j.joei.2020.04.009
17. Bissett, E.J.: Mathematical model of the thermal regeneration of a wall-flow monolith diesel particulate filter. Chem. Eng. Sci. **39**, 1233–1244 (1984). https://doi.org/10.1016/0009-2509(84)85084-8
18. Lee, S.-J., Jeong, S.-J., Kim, W.-S.: Numerical design of the diesel particulate filter for optimum thermal performances during regeneration. Appl. Energy. **86**, 1124–1135 (2009). https://doi.org/10.1016/j.apenergy.2008.07.002
19. Li, Z., Huang, Q., Wang, N.: Pressure drop of asymmetric diesel particulate filter and its influencing factors. Trans. of CSICE. **34**(02), 135–141 (2016)
20. Iwata, H., Konstandopoulos, A., Nakamura, K., Ogiso, A., Ogyu, K., Shibata, T., Ohno, K.: Further experimental study of asymmetric plugging layout on dpfs: effect of wall thickness on pressure drop and soot oxidation. Presented at the SAE Technical Paper. 2015-01-1016 (2015)
21. Zhang, X., Tennison, P., Ruona, W.: 3D numerical study of pressure loss characteristics and filtration efficiency through a frontal unplugged DPF. SAE Int. J. Fuels Lubr. **3**, 177–193 (2010). https://doi.org/10.4271/2010-01-0538
22. Xiao, G., Li, B., Tian, H., Leng, X., Long, W.: Numerical study on flow and pressure drop characteristics of a novel type asymmetric wall-flow diesel particulate filter. Fuel. **267**, 117148 (2020). https://doi.org/10.1016/j.fuel.2020.117148
23. Watling, T.C.: T.C.: A one-dimensional model for square and octo-square asymmetric particulate filters with correct description of the channel and wall geometry. SAE Technical Paper. 2018-01-0951 (2018)
24. Kays, W.M.: Loss coefficients for abrupt changes in flow cross section with low Reynolds number flow in single and multiple-tube systems. J. Fluids Eng. **72**, 1067–1074 (1950)
25. Nakamura, K., Konstandopoulos, A., Kostoglou, M., Shibata, T., Hashizume, Y.: New asymmetric plugging layout of diesel particulate filters for the pressure drop reduction. Presented at the SAE 2014 World Congress. 2014-01-1512 (2014)
26. Bissett, E.J., Kostoglou, M., Konstandopoulos, A.G.: Frictional and heat transfer characteristics of flow in square porous tubes of wall-flow monoliths. Chem. Eng. Sci. **84**, 255–265 (2012). https://doi.org/10.1016/j.ces.2012.08.012
27. Kostoglou, M., Bissett, E.J., Konstandopoulos, A.G.: Improved transfer coefficients for wall-flow monolithic catalytic reactors: energy and momentum transport. Ind. Eng. Chem. Res. **51**, 13062–13072 (2012). https://doi.org/10.1021/ie3011098
28. Konstandopoulos, A.G., Kostoglou, M.: Analysis of asymmetric and variable cell geometry wall-flow particulate filterS. SAE Int. J. Fuels Lubr. **7**, 489–495 (2014). https://doi.org/10.4271/2014-01-1510
29. Luo, J., Tie, Y., Tang, L., Li, Y., Xu, H.: Effect of regeneration method and ash deposition on diesel particulate filter performance: a review. Environ. Sci. Pollut. Res. **30**(16), 45607–45642 (2023)
30. Li, S., Wang, X., Liu, Z.: Study on reaction kinetics of soot oxidation in O_2/CO_2 atmosphere. Jour. Chin. Soc. Pow. Eng. **37**(08), 673–678 (2017)